

## On-Chip Parametric Synchronization of a Dissipative Kerr Soliton Microcomb

Grégory Moille<sup>1,2,\*</sup>, Pradyoth Shandilya<sup>3</sup>, Miro Erkintalo<sup>4,5</sup>, Curtis R. Menyuk<sup>3</sup>, and Kartik Srinivasan<sup>1,2</sup>

<sup>1</sup>*Joint Quantum Institute, NIST/University of Maryland, College Park, Maryland, 20742, USA*

<sup>2</sup>*Microsystems and Nanotechnology Division, National Institute of Standards and Technology, Gaithersburg, Maryland, 20899, USA*

<sup>3</sup>*University of Maryland, Baltimore County, Baltimore, Maryland, 21250, USA*

<sup>4</sup>*Department of Physics, University of Auckland, Auckland 1010, New Zealand*

<sup>5</sup>*The Dodd-Walls Centre for Photonic and Quantum Technologies, Auckland 1010, New Zealand*

 (Received 10 September 2024; revised 16 December 2024; accepted 14 April 2025; published 13 May 2025)

Synchronization of oscillators is ubiquitous in nature. Often, the synchronized oscillators couple directly, yet in some cases synchronization can arise from their parametric interactions. Here, we theoretically predict and experimentally demonstrate the parametric synchronization of a dissipative Kerr soliton frequency comb. We specifically show that the parametric interaction between the soliton and two auxiliary lasers permits the entrainment of the frequency comb repetition rate. Besides representing the first prediction and demonstration of parametric synchronization of soliton frequency combs, our scheme offers significant flexibility for all-optical metrological-scale stabilization of the comb.

DOI: [10.1103/PhysRevLett.134.193802](https://doi.org/10.1103/PhysRevLett.134.193802)

**Introduction**—Synchronization is ubiquitous in nature, from coupled pendulums [1] to fireflies [2], neurons [3], and quantum systems [4,5]. Despite their drastic differences, these systems' synchronization dynamics typically follow common universal patterns and are, to first order, governed by the same mathematical equations. In optics, the same is true for dissipative Kerr solitons (DKSs), which are cornerstones for the creation of on-chip frequency combs [6]. Synchronization between DKSs has been demonstrated, for instance, between counterpropagative solitons [7], or solitons existing in remote resonators [8]. Recently, it has also been shown that a DKS can synchronize to an external continuous-wave reference optical field [9,10], following the same Adler model as coupled oscillators [9,11]. In this Kerr-induced synchronization (KIS) regime, the phase locking of the DKS results in the capture of one comb tooth by the reference field [9,12]. Since the main pump creating the DKS is also a comb tooth, KIS provides a passive dual pinning of the DKS frequency comb, enabling low-noise operation of the microcomb below the fundamental limit imposed by the resonator thermorefractive noise [13], which is critical for metrology applications such as timekeeping [14], time transfer [15], ranging [16], or spectroscopy [17,18]. Although KIS can occur at any comb tooth [10], efficient synchronization requires that the reference laser is both close to a comb line and on resonance, which is challenging to achieve simultaneously due to dispersion, particularly for large frequency separations between the main and reference pumps, which is desirable for optical frequency division (OFD) and clockworks [9].

In this work, we leverage a Kerr parametric interaction driven by two reference lasers to obtain a new DKS synchronization regime that bypasses the above limitation. Related parametric processes have recently attracted significant attention, e.g., for all-optical random number generation [19] and optical spin glasses [20], or for obtaining a new type of parametrically driven dissipative soliton [21]. However, this type of parametric interaction has yet to be explored in the context of DKS synchronization. We show for the first time that the interaction between two on-resonance auxiliary lasers, outside of the DKS comb frequency grid, along with the DKS comb itself, can yield a parametric driving force for the soliton that mediates synchronization. We theoretically unveil the conditions for efficiently obtaining this “parametric KIS,” finding that the resonator must exhibit at least third-order dispersion to support a zero crossing of the integrated dispersion. Experimentally, we demonstrate this effect using an octave-spanning comb in a Si<sub>3</sub>N<sub>4</sub> microring resonator. Similar to standard KIS [9], parametric KIS stabilizes the microcomb, such that its repetition rate becomes dependent on the three lasers at play.

**Results**—First, we present the theoretical framework of the novel parametric-KIS scheme. The system consists of a microring resonator that is triply pumped [Fig. 1(a)]. The intracavity field  $a(\theta, t)$  can be modeled using a modified Lugiato-Lefever equation (mLLE) [22]:

$$\begin{aligned} \frac{\partial a(\theta, t)}{\partial t} = & \left( -\frac{\kappa}{2} + i\Delta\omega_0 \right) a + i \sum_{\mu} D_{\text{int}}(\mu) A(\mu, t) e^{i\mu\theta} \\ & - i\gamma |a|^2 a + iF_0 \\ & + iF_- e^{i\varpi_- t + i\mu_- \theta} + iF_+ e^{i\varpi_+ t + i\mu_+ \theta}, \end{aligned} \quad (1)$$

\*Contact author: gmoille@umd.edu

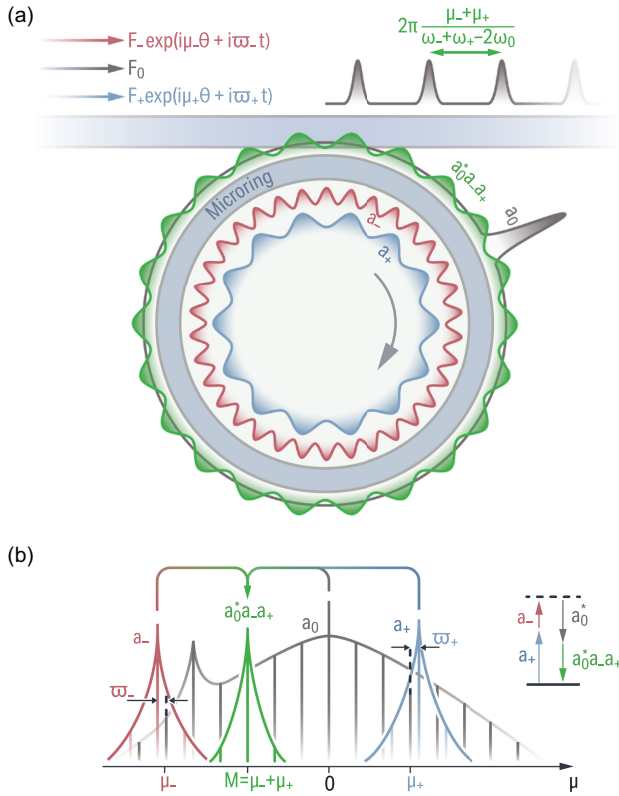


FIG. 1. (a) Schematic of the parametric-KIS system. A main pump  $F_0$  generates a DKS  $a_0$ . Two additional drives  $F_{\pm}$  at mode indices  $\mu_{\pm}$  and relative frequency offset  $\varpi_{\pm}$  from their nearest DKS comb tooth are injected into the same resonator to create the two other colors  $a_{-}$  and  $a_{+}$ . The parametric interaction between the three colors  $a_0$ ,  $a_{-}$ , and  $a_{+}$  creates a parametric drive for  $a_0$ , which when in phase with the DKS can synchronize it. Thus, it disciplines the pulse train repetition rate. (b) Spectral representation of the same system as in (a) where each comb component is frequency offset by  $\varpi_{\pm}$  respectively, highlighting how the parametric drive at  $M = \mu_{-} + \mu_{+}$  provides the optical frequency division factor.

where  $\theta$  is the azimuthal coordinate that rotates with the DKS angular group velocity,  $t$  is time,  $\mu$  is the mode difference with respect to the mode of the primary pump, and  $A(\mu, t)$  is the Fourier transform of  $a(\theta, t)$ . The parameters  $\kappa$ ,  $\Delta\omega_0 = \omega_{\text{res}}(0) - \omega_0$ , and  $\gamma$  denote the total loss rate, the offset between the primary pump  $\omega_0$  and the primary pump resonance  $\omega_{\text{res}}(0)$ , and the Kerr coefficient, respectively. The parameter  $F_0$  is related to the primary pump power  $P_0 = F_0^2/\kappa_{\text{ext}}$ , where  $\kappa_{\text{ext}}$  is the coupling loss rate. We similarly define  $F_{\pm}$  via the relations  $P_{\pm} = F_{\pm}^2/\kappa_{\text{ext}}$ . The modified integrated dispersion, which we define with the DKS repetition rate outside of synchronization  $\omega_{\text{rep}}^{(0)}$  instead of the angular free spectral range around the pump resonance  $D_1$ , is  $D_{\text{int}}(\mu) = \omega_{\text{res}}(\mu) - (\omega_{\text{res}}(0) + \mu\omega_{\text{rep}}^{(0)}) = (D_1 - \omega_{\text{rep}}^{(0)})\mu + \sum_{k>1} D_k \mu^k/k!$ , where  $\omega_{\text{res}}(\mu)$  is the frequency of resonance at mode  $\mu$ , and  $D_k$  the higher order dispersion terms. The two auxiliary pumps

are at frequencies  $\omega_{\pm}$  and are located at modes  $\mu_{\pm}$  with respect to the primary pump, such that  $\mu_{-} < 0$  and  $\mu_{+} > 0$ . These pumps are offset from their nearest comb tooth by  $\varpi_{\pm} = \omega_{\pm} - \omega_0 - \mu\omega_{\text{rep}}^{(0)}$ .

In the regime of interest to us here, the integrated dispersion is sufficiently small for a three-component multicolor soliton (McS) to form [23,24]. The McS consists of the DKS and two azimuthally localized structures with carrier frequencies  $\omega_{\pm}$  that are locked to each other in group (but not phase) velocity, leading to different accumulated phase shifts at each round trip. In the frequency domain, the McS is associated with three interleaved frequency combs that share the same repetition rate  $\omega_{\text{rep}}$  but are offset from one another, with  $\varpi_{\pm}$  representing the offset of the combs around the auxiliary pump frequencies from the DKS comb [Fig. 1(b)]. Standard KIS is achieved by tuning  $\varpi_{+}$  or  $\varpi_{-}$  to be small, such that the corresponding pump captures a comb tooth, at which point the colors generated by the two pumps become indistinguishable [9]. In stark contrast, in the parametric-KIS regime explored in this work, the parameters  $\varpi_{\pm}$  are generally large such that standard KIS does not occur. In this case, and similar to Ref. [24], the total intracavity field can be expanded as a superposition of the three colors, viz.

$$a(\theta, t) = a_0(\theta, t) + a_{-}(\theta, t)e^{i(\varpi_{-}t + \mu_{-}\theta)} + a_{+}(\theta, t)e^{i(\varpi_{+}t + \mu_{+}\theta)}. \quad (2)$$

After some algebra detailed in Supplemental Material, S.1 [25], Eqs. (1) and (2) lead to the DKS equation:

$$\begin{aligned} \frac{\partial a_0(\theta, t)}{\partial t} = & \left( -\frac{\kappa}{2} + i\Delta\omega_0 \right) a_0 + i \sum_{\mu} D_{\text{int}}(\mu) A_0(\mu, t) e^{i\mu\theta} \\ & - i\gamma(2|a_{-}|^2 + |a_0|^2 + 2|a_{+}|^2) a_0 \\ & - i2\gamma a_0^* a_{+} a_{-} e^{i(Wt + M\theta)} + iF_0, \end{aligned} \quad (3)$$

where  $W = \varpi_{-} + \varpi_{+}$  is the frequency offset of the idler wave that is generated via the parametric interaction from its closest DKS comb line at mode  $M = \mu_{-} + \mu_{+}$ . Equation (3) is similar to the master equation of the  $\chi^{(3)}$ -mediated parametric soliton [21], except with an additional direct driving force  $F_0$ ; Eq. (3) is also similar to the equation used to study standard KIS of DKSs [9], but now with a parametric synchronization term  $2\gamma a_0^* a_{+} a_{-}$  from the four-wave mixing between the reference fields  $a_{\pm}$  and the soliton  $a_0$ , which concomitantly generates an idler field at  $\omega_{+} + \omega_{-} - \omega_0$ .

Hence, we may anticipate that the DKS in the triply driven scheme shown in Fig. 1(a) can experience synchronization, provided that the parametric driving term is sufficiently close in phase with the DKS. Indeed, a detailed analysis shows that, similar to any other synchronization mechanism for coupled oscillators, parametric KIS obeys

an Adler equation (see Supplemental Material, S.2 [25]), where  $W$  is compensated by a temporal phase-slip of the DKS to achieve phase locking. The analysis (detailed in the Supplemental Material, S.1 [25]) leading to Eq. (3) also shows that, when parametrically synchronized, the comb exhibits the OFD factor  $M = \mu_- + \mu_+$  which, contrary to direct KIS, arises from the nonlinear interaction between the three colors. Therefore, parametric KIS enables for a triple pinning of the repetition rate from degenerated four-wave mixing, in contrast with the direct-KIS dual pinning:

$$\omega_{\text{rep}}^{(\text{pkis})} = \frac{\omega_- + \omega_+ - 2\omega_0}{M}. \quad (4)$$

Although off-resonance operation of the auxiliary pumps (as in direct KIS [10]) is possible, the efficiency of parametric KIS is optimized when the pumps are on resonance to maximize their respective intracavity powers, while allowing for  $|W|$  to be minimized. Such a condition exists if  $D_{\text{int}}(\mu_-) \approx -D_{\text{int}}(\mu_+)$ . Thus, to achieve on-resonance parametric-KIS operation, the resonator should have at least one zero crossing in its integrated dispersion  $D_{\text{int}}(\mu)$ , and therefore should exhibit at least a non-negligible  $D_3$  term.

We demonstrate parametric KIS numerically by solving Eq. (3) along with the equation describing  $a_-$  and  $a_+$  (see Supplemental Material, S.1 [25]), using an integrated dispersion described by a cubic function with  $D_2/2\pi = 21$  MHz and  $D_3/2\pi = 1.25$  MHz, and assuming  $D_1/2\pi = 983.346$  GHz. The DKS with  $\omega_{\text{rep}}/2\pi = 983.515$  GHz, different from  $D_1$  because of dispersive wave (DW) recoil [26], is generated by a main pump with power  $P_0 = 150$  mW and detuning  $\Delta\omega_0/2\pi = -3.2$  GHz in a system where  $\kappa_{\text{ext}} = \kappa/2 = 2\pi \times 200$  MHz for critical coupling condition. The modified integrated dispersion presents a zero crossing at  $\mu = -53$  [Fig. 2(a)], where  $a_0$  exhibits the creation of a dispersive wave. We choose the auxiliary pumps, with power  $P_- = 1$  mW and  $P_+ = 3$  mW, respectively, at  $\mu_- = -57$  and  $\mu_+ = 25$  for the components  $a_-$  and  $a_+$  to exhibit, while on resonance, relative offsets that are almost equal with opposite signs  $-\varpi_-/2\pi \approx \varpi_+/2\pi \approx 10$  GHz. By fine tuning the frequency detunings  $\delta\omega_{\pm}$  of the auxiliary pumps, the frequency offset  $W$  between the parametrically generated idler field and a DKS comb tooth can be pushed to lie within the parametric-KIS bandwidth (i.e.,  $\lesssim 1$  GHz). Additionally, the colors  $a_-$  and  $a_+$ , which are not phase synchronized with  $a_0$ , experience the creation of additional azimuthal tones, regardless of their dispersion regime, thanks to the group-velocity binding of all the colors through cross-phase modulation (XPM) [27–29]. The parametric driving force that synchronizes the DKS and which results from the three colors can be numerically extracted, exhibiting a clear tone at  $M = \mu_- + \mu_+ = -32$  at the  $a_0$  color, i.e.,  $|W| \ll |\varpi_{\pm}|$ , as expected by the theory. The azimuthal profile of  $a_0$  with respect to time allows us to

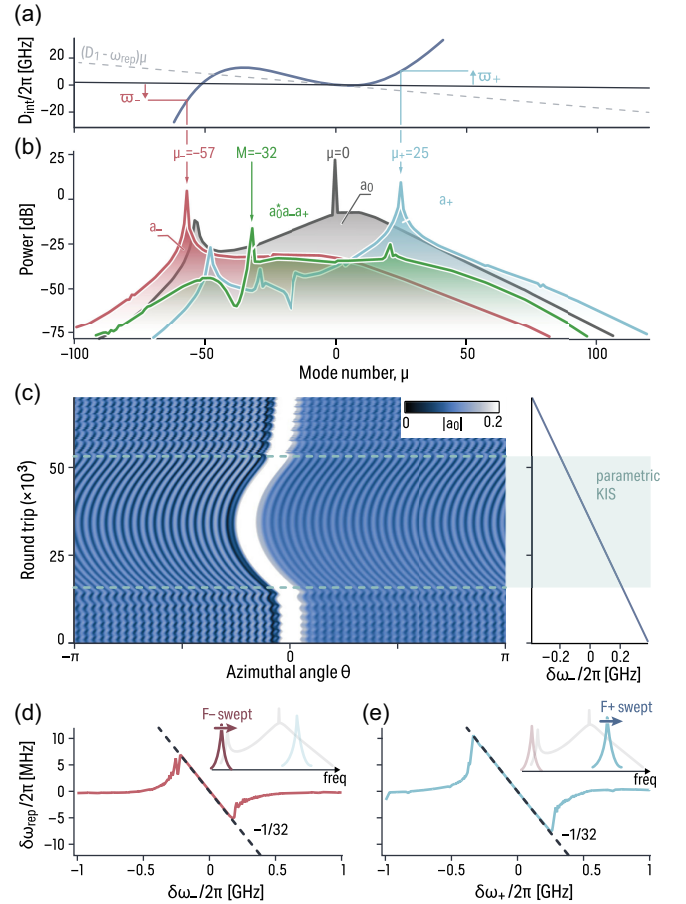


FIG. 2. (a) Modified integrated dispersion  $D_{\text{int}}(\mu)$  of the resonator used in the simulation. (b) Simulated comb spectrum for the three colors at play: the DKS'  $a_0$  (gray) and both auxiliaries'  $a_{\pm}$  with  $\mu_- = -57$  (red) and  $\mu_+ = 25$  (blue). The resulting parametric driving field for the DKS' color  $a_0$  is then at  $M = \mu_- + \mu_+ = -32$  (green). (c) Azimuthal profile (left, color scale) of the DKS color with respect to the negative auxiliary pump detuning  $\delta\omega_-$  (right). Outside of KIS, the parametric drive has an offset leading to a phase slip in time relative to the DKS, resulting in a CEO offset in the frequency domain. Once synchronized, their phase velocities lock and the variation of  $W$  entrains the DKS's and hence disciplines its repetition rate, as apparent through its azimuthal drift. (d),(e) Repetition rate variation  $\delta\omega_{\text{rep}}$  of the DKS with respect to the detuning of the negative (d) and positive (e) auxiliary pump detuning  $\delta\omega_-$  and  $\delta\omega_+$ , respectively. Once the parametric KIS is reached,  $\delta\omega_{\text{rep}}$  varies with the OFD  $M = \mu_- + \mu_+$ , accordingly with Eq. (4).

understand the synchronization mechanism [Fig. 2(c)]. Outside of synchronization, the parametric term exhibits a phase slip  $Wt \pmod{2\pi}$  from the DKS, resulting in a nonstationary interference pattern, equivalent to a CEO offset in the frequency domain. Once the parametric KIS is reached and synchronization is achieved, the  $a_0^* a_- a_+$  driving term becomes in phase with the DKS, hence the absence of modulation of the azimuthal profile in time.

While synchronized, a change in frequency of either auxiliary pump leads to a phase change of the synchronized

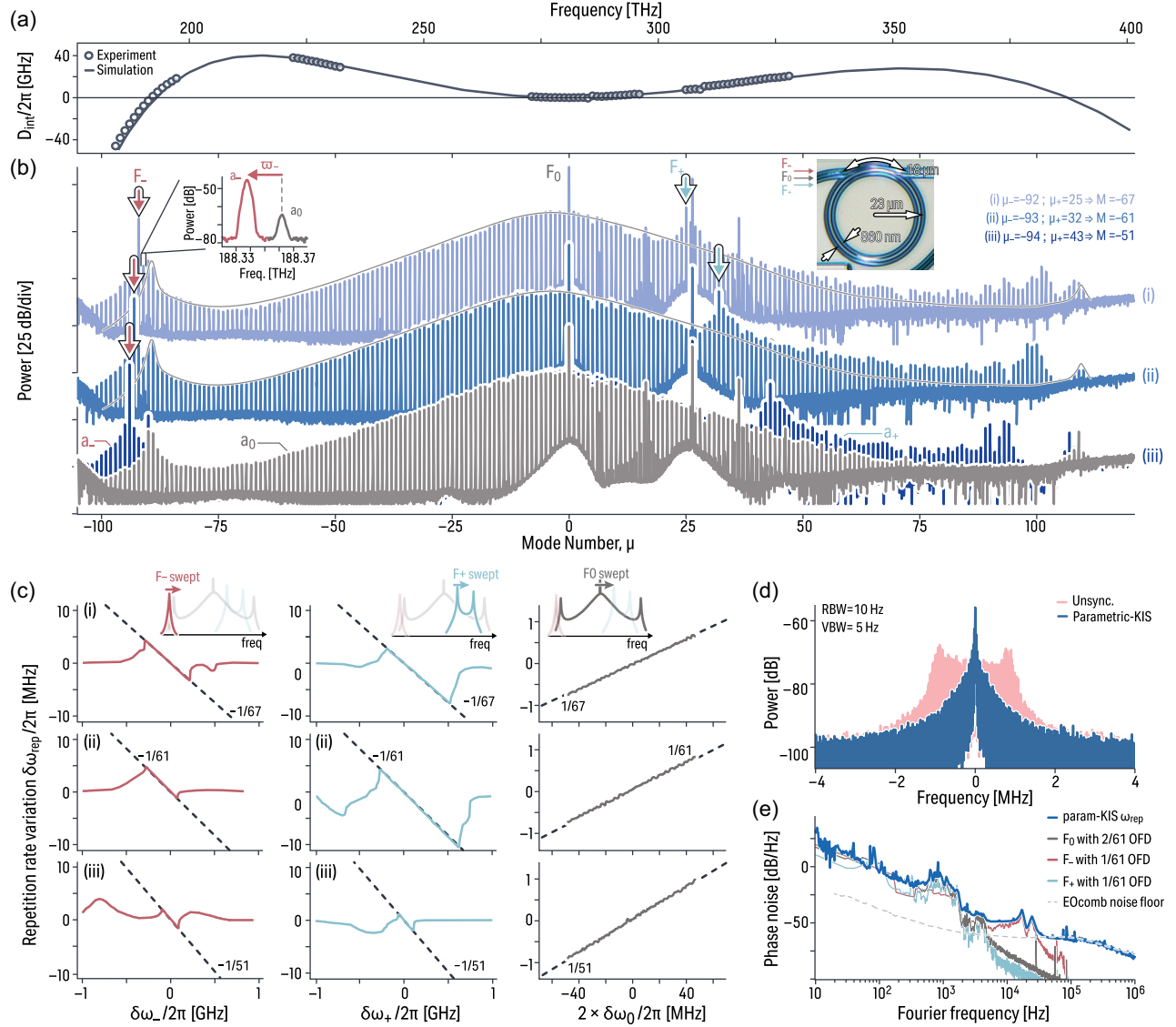


FIG. 3. (a) Integrated dispersion measurement (open circles) and simulation (solid line) for the microring resonator under study. (b) Frequency comb optical spectra in parametric KIS for different OFD factors, from top to bottom,  $M = -67$ ,  $-61$ , and  $-51$ . The left inset highlights the frequency offset  $\omega_-$  between the components  $a_-$  and  $a_0$ . The soliton color  $a_0$  is displayed in gray and remains the same for each  $\mu_{\pm}$  configuration (gray envelope). The right inset shows a microscope image of the microring and its critical dimensions. (c) Repetition rate disciplining for (i)  $M = -67$ , (ii)  $-61$ , and (iii)  $-51$ , where  $\delta\omega_-$  (left),  $\delta\omega_+$  (center), and  $\delta\omega_0$  (right) is swept. In the case of  $\delta\omega_0$  sweep, we account for a factor 2 in the detuning due to the parametric nature of the process [see Eq. (4)]. Only a small excursion within the parametric KIS is shown for the main pump to avoid disrupting the DKS. (d) Electrical spectra of the repetition rate beat when the DKS is free running (pink) and parametrically synchronized (blue). RBW: resolution bandwidth; VBW: video bandwidth. The power is normalized to 1 mW, equivalent to decibel-milliwatts. (e) Phase noise of the repetition rate (blue thick) in the parametric-KIS regime, with the different noise contributions of each pump according to Eq. (4) displayed, highlighting the repetition rate optical frequency divided from the pump noises. The EOcomb apparatus (dash line) defines the noise floor of the repetition rate measurement. The power is normalized to the carrier's, equivalent to dBc/Hz.

DKS, causing a drift in its position in time and thus its repetition rate. However, none of the auxiliary pumps directly capture any comb teeth, which is in stark contrast with direct KIS [9] or other color KIS [29] schemes. We can extract the repetition rate change  $\delta\omega_{\text{rep}}$  of  $a_0$ , which through XPM is the same as  $a_{\pm}$ , and study its entrainment with the auxiliary pumps' frequency change  $\delta\omega_{\pm}$ . As expected from

Eq. (4) in the parametric-KIS regime, we obtain  $\delta\omega_{\text{rep}}/\delta\omega_- = \delta\omega_{\text{rep}}/\delta\omega_+ = 1/M$  [Figs. 2(d) and 2(e)]. We also confirm such results with different  $\mu_{\pm}$  combinations (see Supplemental Material, S.6 [25]), where unlike direct KIS, which allows efficient resonant operation only at the DW, parametric KIS allows it at any  $\mu_{\pm}$  pairs where  $D_{\text{int}}(\mu_-) = -D_{\text{int}}(\mu_+)$ . In this context, parametric KIS

enables more efficient synchronization at the off-resonance comb tooth  $M$  than direct KIS with comparable reference powers (see Supplemental Material, S.8 [25]). This occurs due to the near-resonant input fields driving an efficient nondegenerate four-wave mixing process that produces large intracavity power at an (off-resonant) idler frequency to capture that  $M$  th comb tooth.

We now proceed to demonstrate parametric KIS experimentally. We use an integrated microring resonator with a radius of  $R = 23 \mu\text{m}$ , made of  $H = 670 \text{ nm}$  thick  $\text{Si}_3\text{N}_4$ , and a ring width of  $RW = 860 \text{ nm}$  embedded in  $\text{SiO}_2$ . The bus waveguide is configured in a pulley fashion with a length  $L_c = 18 \mu\text{m}$ , compensating for the coupling dispersion [30] and allowing for efficient extraction of the entire comb. We pump the microring at a frequency  $\omega_0/2\pi \approx 281.3 \text{ THz}$  with an on-chip power  $P_0 = 180 \text{ mW}$  to generate an octave-spanning soliton microcomb at  $\omega_{\text{rep}}/2\pi = 999.60376 \text{ GHz}$  ( $\pm 10 \text{ kHz}$ ), while using a cooler laser at  $\approx 308 \text{ THz}$  to thermally stabilize the system [31,32]. The comb exhibits two DWs [Fig. 3(b)] at  $\mu = -90$  (191.3 THz) and  $\mu = 108$  (389 THz), due to the two zero crossings of  $D_{\text{int}}(\mu)$  [Fig. 3(a)]. As described earlier, zero crossings lead to resonant modes  $\mu_{\pm}$  that when pumped by auxiliary lasers, create colors  $a_{\pm}$  with opposite phases  $\varpi_{+} \approx -\varpi_{-}$ . Such mode combinations can be found under dual pumping, where the  $a_{-}$  color creates through nonlinear mixing a third color for which phase matching will be at  $\mu_{+}$  (and vice versa) [23,24]. In our experiment, such conditions, along with equipment compatibility, are met at  $\{\mu_{-}; \mu_{+}\} = \{-92; 25\}$ ,  $\{-93; 32\}$ , and  $\{-94; 43\}$ , resulting in an OFD of  $M = -67, -61, \text{ and } -51$  [Fig. 3(b)]. For all the experiments, the on-chip powers of the auxiliary pumps are set to  $P_{-} = 1.25 \text{ mW}$  and  $P_{+} = 2.75 \text{ mW}$ . We record the DKS repetition rate using an electro-optic comb apparatus similar to Refs. [9,29,33] (see Supplemental Material, S.5 [25]). The parametric KIS is detected by recording the temporal trace of the EO-comb frequency down-converted  $\omega_{\text{rep}}$  while only one of the pump laser frequencies is swept. Once processed (see Supplemental Material, S.5 [25]), this enables us to retrieve the dependence of  $\omega_{\text{rep}}$  on the laser detuning [Fig. 3(c)].

We confirm the parametric nature of such Kerr-induced synchronization since we obtain the  $\omega_{\text{rep}}$  entrainment, similar to the simulation, for  $\delta\omega_{\text{rep}}/\delta\omega_{-} = \delta\omega_{\text{rep}}/\delta\omega_{+} = 1/M$  for each of the  $\mu_{\pm}$  pairs under study. We note the difference in parametric KIS bandwidth from the  $\mu_{\pm}$  auxiliary pumps, which we believe arises from the remaining  $\kappa_{\text{ext}}$  dispersion, impacting the  $F_{-}$  and  $F_{+}$  driving forces. A unique feature of the parametric KIS, deduced from Eq. (4), is the double contribution from the main pump. While in parametric KIS, we change the main pump frequency by  $\delta\omega_0$ —different from  $\Delta\omega_0$  since the cooler pump thermally stabilizes the detuning from the resonance—and we observe a disciplining  $\delta\omega_{\text{rep}}/\delta\omega_0 = -2/M$ , as expected from the theory.

Finally, we characterize the parametrically synchronized DKS noise. Like direct KIS, the pinned repetition rate shows significantly reduced noise compared to the untrapped case [Fig. 3(d)]. Measurements of the repetition rate phase noise power spectral density (PSD) verify the parametric-KIS OFD. Using an optical frequency discriminator (see Supplemental Material, S.5 [25]), we find the repetition rate phase noise PSD matches the combined contribution of the three free-running lasers' phase noise PSD according to Eq. (4) [Fig. 3(e)], where the repetition rate detection is limited only by the EO comb apparatus noise floor used for spectrally translating two DKS comb teeth into a detectable frequency. Since our OFD is competitive with state-of-the-art two-point locked microcombs for low-noise microwave generation [34–36], we expect similar performances when the three lasers would be locked to frequency references.

*Discussion*—In conclusion, we have demonstrated that harnessing the  $\chi^{(3)}$  nonlinearity of a microresonator housing a dissipative Kerr soliton enables parametric Kerr-induced synchronization using two auxiliary lasers injected outside the soliton microcomb's frequency grid. As a result, the soliton is trapped in the field that is generated by the parametric interaction of different colors in the cavity. We have shown that this effect can be predicted by the multicolor formalism of the LLE, where the parametric interaction between the different waves gives rise to an additional force to the soliton color. We have numerically and experimentally demonstrated this effect, stabilizing the microcomb with auxiliary lasers outside the DKS microcomb's frequency grid. Additionally, other colors beyond the DKS can undergo parametric synchronization with suitable auxiliary pumping (see Supplemental Material, S.7 [25]). Leveraging the group velocity binding for DKS stabilization through dual pinning of another color [29], this scheme offers enhanced flexibility for all-optical locking while relaxing the dispersion requirements for on-resonance operation compatible with pure quadratic  $D_{\text{int}}$ . Our work presents the first prediction and demonstration of parametric synchronization of a DKS microcomb, opening new pathways for studying and applying the trapping of DKSs without direct actuation. It is important to note that parametric driving of solitons is not limited to  $\chi^{(3)}$  systems [37,38]. Thus, the parametric KIS of a DKS could be extended to other nonlinear orders, with potentially significant implications for the dual-pinning and noise of the frequency comb. Additionally, our work presents the potential for using multicolor solitons in metrology, harnessing their spectral extension [23] beyond the resonator's anomalous dispersion limit.

*Acknowledgments*—G. M., K. S., and M. E. acknowledge partial funding support from Marsden Fund of the Royal Society Te Apārangi [Grant No. 23-UOA-071]. G. M. and K. S. acknowledge partial funding support from

the Space Vehicles Directorate of the Air Force Research Laboratory and the NIST-on-a-chip program of the National Institute of Standards and Technology. P. S. and C. M. acknowledges support from the Air Force Office of Scientific Research (Grant No. FA9550-20-1-0357), the National Science Foundation (Grant No. ECCS-18-07272), and by a collaborative agreement 2022138-142232 and 2023200-142386 with the National Center for Manufacturing Sciences as a subaward from U.S. DoD cooperative agreement HQ0034-20-2-0007. We thank Logan Courtright and Usman Javid for insightful feedback. G. M. thanks T. B. M. for feedback and support.

- 
- [1] S. Strogatz, *SYNC: The emerging science of spontaneous order* (Penguin, UK, 2004).
- [2] J. Buck and E. Buck, Mechanism of rhythmic synchronous flashing of fireflies, *Science* **159**, 1319 (1968).
- [3] J. Fell and N. Axmacher, The role of phase synchronization in memory processes, *Nat. Rev. Neurosci.* **12**, 105 (2011).
- [4] A. K. Jain, K. K. Likharev, J. E. Lukens, and J. E. Sauvageau, Mutual phase-locking in Josephson junction arrays, *Phys. Rep.* **109**, 309 (1984).
- [5] B. Militello, H. Nakazato, and A. Napoli, Synchronizing quantum harmonic oscillators through two-level systems, *Phys. Rev. A* **96**, 023862 (2017).
- [6] T. J. Kippenberg, A. L. Gaeta, M. Lipson, and M. L. Gorodetsky, Dissipative Kerr solitons in optical microresonators, *Science* **361**, eaan8083 (2018).
- [7] Q.-F. Yang, X. Yi, K. Y. Yang, and K. Vahala, Counter-propagating solitons in microresonators, *Nat. Photonics* **11**, 560 (2017).
- [8] J. K. Jang, A. Klenner, X. Ji, Y. Okawachi, M. Lipson, and A. L. Gaeta, Synchronization of coupled optical microresonators, *Nat. Photonics* **12**, 688 (2018).
- [9] G. Moille, J. Stone, M. Chojnacky, R. Shrestha, U. A. Javid, C. Menyuk, and K. Srinivasan, Kerr-induced synchronization of a cavity soliton to an optical reference, *Nature (London)* **624**, 267 (2023).
- [10] T. Wildi, A. Ulanov, N. Englebort, T. Voumard, and T. Herr, Sideband injection locking in microresonator frequency combs, *APL Photonics* **8**, 120801 (2023).
- [11] P. Couillet, J. M. Gilli, M. Monticelli, and N. Vandenberghe, A damped pendulum forced with a constant torque, *Am. J. Phys.* **73**, 1122 (2005).
- [12] T. Wildi, A. E. Ulanov, T. Voumard, B. Ruhnke, and T. Herr, Phase-stabilised self-injection-locked microcomb, *Nat. Commun.* **15**, 7090 (2024).
- [13] G. Moille, P. Shandilya, J. Stone, C. Menyuk, and K. Srinivasan, All-optical noise quenching of an integrated frequency comb, [arXiv:2405.01238](https://arxiv.org/abs/2405.01238).
- [14] S. T. Cundiff and J. Ye, Colloquium: Femtosecond optical frequency combs, *Rev. Mod. Phys.* **75**, 325 (2003).
- [15] E. D. Caldwell, J.-D. Deschenes, J. Ellis, W. C. Swann, B. K. Stuhl, H. Bergeron, N. R. Newbury, and L. C. Sinclair, Quantum-limited optical time transfer for future geosynchronous links, *Nature (London)* **618**, 721 (2023).
- [16] H. Zhang, H. Wei, H. Yang, and Y. Li, Active laser ranging with frequency transfer using frequency comb, *Appl. Phys. Lett.* **108**, 181101 (2016).
- [17] B. J. Bjork, T. Q. Bui, O. H. Heckl, P. B. Changala, B. Spaun, P. Heu, D. Follman, C. Deutsch, G. D. Cole, M. Aspelmeyer, M. Okumura, and J. Ye, Direct frequency comb measurement of  $\text{OD} + \text{CO} \rightarrow \text{DOCOCO}$  kinetics, *Science* **354**, 444 (2016).
- [18] R. Holzwarth, T. Udem, T. W. Hänsch, J. C. Knight, W. J. Wadsworth, and P. St. J. Russell, Optical frequency synthesizer for precision spectroscopy, *Phys. Rev. Lett.* **85**, 2264 (2000).
- [19] Y. Okawachi, M. Yu, K. Luke, D. O. Carvalho, M. Lipson, and A. L. Gaeta, Quantum random number generator using a microresonator-based Kerr oscillator, *Opt. Lett.* **41**, 4194 (2016).
- [20] Y. Okawachi, M. Yu, J. K. Jang, X. Ji, Y. Zhao, B. Y. Kim, M. Lipson, and A. L. Gaeta, Demonstration of chip-based coupled degenerate optical parametric oscillators for realizing a nanophotonic spin-glass, *Nat. Commun.* **11**, 4119 (2020).
- [21] G. Moille, M. Leonhardt, D. Paligora, N. Englebort, F. Leo, J. Fatome, K. Srinivasan, and M. Erkintalo, Parametrically driven pure-Kerr temporal solitons in a chip-integrated microcavity, *Nat. Photonics* **18**, 617 (2024).
- [22] H. Taheri, A. B. Matsko, and L. Maleki, Optical lattice trap for Kerr solitons, *Eur. Phys. J. D* **71**, 153 (2017).
- [23] G. Moille, E. F. Perez, J. R. Stone, A. Rao, X. Lu, T. S. Rahman, Y. K. Chembo, and K. Srinivasan, Ultra-broadband Kerr microcomb through soliton spectral translation, *Nat. Commun.* **12**, 7275 (2021).
- [24] C. R. Menyuk, P. Shandilya, L. Courtright, G. Moille, and K. Srinivasan, Multi-color solitons and frequency combs in microresonators, [arXiv:2409.03880](https://arxiv.org/abs/2409.03880).
- [25] See Supplemental Material at <http://link.aps.org/supplemental/10.1103/PhysRevLett.134.193802> for parametric trapping of colors other than the primary DKS, a comparison of parametric KIS and direct KIS, and additional details regarding experiments, theory, and simulations.
- [26] A. V. Cherenkov, V. E. Lobanov, and M. L. Gorodetsky, Dissipative Kerr solitons and Cherenkov radiation in optical microresonators with third-order dispersion, *Phys. Rev. A* **95**, 033810 (2017).
- [27] Y. Wang, F. Leo, J. Fatome, M. Erkintalo, S. G. Murdoch, and S. Coen, Universal mechanism for the binding of temporal cavity solitons, *Optica* **4**, 855 (2017).
- [28] P. C. Qureshi, V. Ng, F. Azeem, L. S. Trainor, H. G. L. Schwefel, S. Coen, M. Erkintalo, and S. G. Murdoch, Soliton linear-wave scattering in a Kerr microresonator, *Commun. Phys.* **5**, 1 (2022).
- [29] G. Moille, P. Shandilya, A. Niang, C. Menyuk, G. Carter, and K. Srinivasan, Versatile optical frequency division with Kerr-induced synchronization at tunable microcomb synthetic dispersive waves, *Nat. Photonics* **19**, 36 (2025).
- [30] G. Moille, Q. Li, T. C. Briles, S.-P. Yu, T. Drake, X. Lu, A. Rao, D. Westly, S. B. Papp, and K. Srinivasan, Broadband resonator-waveguide coupling for efficient extraction of octave-spanning microcombs, *Opt. Lett.* **44**, 4737 (2019).
- [31] H. Zhou, Y. Geng, W. Cui, S.-W. Huang, Q. Zhou, K. Qiu, and C. Wei Wong, Soliton bursts and deterministic

- dissipative Kerr soliton generation in auxiliary-assisted microcavities, *Light* **8**, 50 (2019).
- [32] S. Zhang, J. M. Silver, L. Del Bino, F. Copie, M. T. M. Woodley, G. N. Ghalanos, A. Ø. Svela, N. Moroney, and P. Del’Haye, Sub-milliwatt-level microresonator solitons with extended access range using an auxiliary laser, *Optica* **6**, 206 (2019).
- [33] T. E. Drake, T. C. Briles, J. R. Stone, D. T. Spencer, D. R. Carlson, D. D. Hickstein, Q. Li, D. Westly, K. Srinivasan, S. A. Diddams, and S. B. Papp, Terahertz-rate Kerr-microresonator optical clockwork, *Phys. Rev. X* **9**, 031023 (2019).
- [34] S. B. Papp, K. Beha, P. Del’Haye, F. Quinlan, H. Lee, K. J. Vahala, and S. A. Diddams, Microresonator frequency comb optical clock, *Optica* **1**, 10 (2014).
- [35] S. Sun, B. Wang, K. Liu, M. W. Harrington, F. Tabatabaei, R. Liu, J. Wang, S. Hanifi, J. S. Morgan, M. Jahanbozorgi, Z. Yang, S. M. Bowers, P. A. Morton, K. D. Nelson, A. Beling, D. J. Blumenthal, and X. Yi, Integrated optical frequency division for microwave and mmWave generation, *Nature (London)* **627**, 540 (2024).
- [36] I. Kudelin *et al.*, Photonic chip-based low-noise microwave oscillator, *Nature (London)* **627**, 534 (2024).
- [37] A. W. Bruch, X. Liu, Z. Gong, J. B. Surya, M. Li, C.-L. Zou, and H. X. Tang, Pockels soliton microcomb, *Nat. Photonics* **15**, 21 (2021).
- [38] N. Englebort, F. De Lucia, P. Parra-Rivas, C. M. Arabí, P.-J. Sazio, S.-P. Gorza, and F. Leo, Parametrically driven Kerr cavity solitons, *Nat. Photonics* **15**, 857 (2021).